Mon. Not. R. Astron. Soc. **000**, 1–8 (2003) Printed 16 September 2003 (MN LaTeX style file v2.2)

XMM-Newton Observations of the Perseus Cluster II: Evidence for Gas Motions in the Core

E. Churazov,[1,2] W. Forman,[3] C. Jones,[3] R.Sunyaev[1,2] and H. Böhringer[4]
[1] *Max-Planck-Institut für Astrophysik, Karl-Schwarzschild-Strasse 1, 85741 Garching, Germany*
[2] *Space Research Institute (IKI), Profsoyuznaya 84/32, Moscow 117810, Russia*
[3] *Harvard-Smithsonian Center for Astrophysics, 60 Garden St., Cambridge, MA 02138, USA*
[4] *MPI für Extraterrestrische Physik, P.O. Box 1603, 85740 Garching, Germany*

16 September 2003

ABSTRACT
The 5-9 keV spectrum of the inner ~100 kpc of the Perseus cluster measured by XMM-Newton can be well described by an optically thin plasma emission model as predicted by the APEC code, without any need for invoking a strong Ni overabundance or the effects of resonant scattering. For the strongest 6.7 keV line of He-like iron, the optical depth of the cluster, calculated using observed density, temperature and abundance profiles, is of order 3. The lack of evidence for resonant scattering effects implies gas motion in the core with a range in velocities of at least half of the sound velocity. If this motion has the character of small scale turbulence, then its dissipation would provide enough energy to compensate for radiative cooling of the gas. The activity of the supermassive black hole at the center of the cluster may be the driving force of the gas motion.

Key words: clusters: individual: Perseus - cooling flows

1 INTRODUCTION

The X-ray emission of the hot gas in galaxy clusters is usually modeled as emission by an optically thin plasma. The assumption that the cluster gas is optically thin is certainly valid for the continuum emission, but for the strongest resonant lines the cluster can be moderately thick (e.g. Gilfanov, Sunyaev & Churazov, 1987). Resonant scattering causes changes in line intensities relative to the continuum, thus affecting measurements of the heavy element abundances (Gilfanov et al. 1987, Shigeyama 1998), and producing polarization of the line flux at the level of ~10% (Sazonov, Churazov & Sunyaev, 2002). For a typical rich cluster one can expect the resonant scattering to be especially important for the He-like iron K_α line at 6.7 keV. It is most convenient to search for resonant scattering effects by comparing the flux from this line with the flux of the He-like iron K_β line at 7.9 keV. In particular, for the Perseus cluster, Molendi et al. (1998) and Akimoto et al. (1997,1999) argued that an anomalously high ratio of the He-like iron K_β and K_α lines hints at the importance of resonant scattering. The 7.9 keV line of iron is however blended with the He-like nickel K_α line and the anomalous line ratio may be interpreted as evidence for an enhanced Ni abundance (Dupke & Arnaud, 2001). The role of resonant scattering also has been discussed for other objects, in particular M87 (Böhringer et al. 2001, Mathews, Buote and Brighenti 2001, Matsushita, Finoguenov & Böhringer 2003) and NGC 4636 (Xu et al., 2002).

Below we use an XMM-Newton 50 ksec observation of the Perseus cluster to assess the possible role of resonant scattering. The detailed description of the data and the analysis procedure are given in Churazov et al. (2003).

The structure of the paper is as follows. In Section 2 we simulate the effect of resonant scattering on the radial profiles of the line intensities. In Section 3 we compare the results of the observations with the simulations. In Section 4 we set a lower limit on the level of gas turbulence, which in the context of this paper means differential gas flows on scales smaller than ~100 kpc. In Section 5 we briefly argue that the central abundance decrement may not be a strong argument in favor of resonant scattering. Implications of turbulent motions on the thermal balance of the gas are discussed in Section 6. The last section summarizes our findings.

Throughout the paper we use $H_0 = 70\ km/s/Mpc$.

2 RESONANT SCATTERING

The radial dependence of the electron density n_e and temperature T_e of the gas in the Perseus cluster is taken from Churazov et al. (2003), rescaled to $H_0 = 70\ km/s/Mpc$,

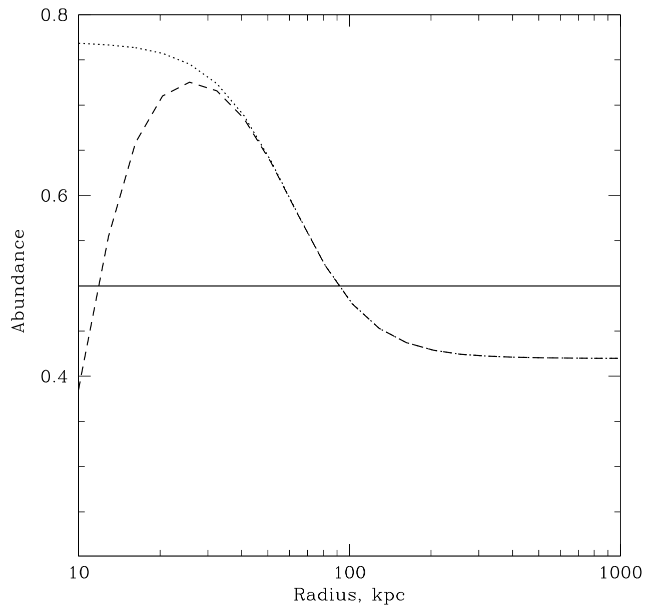

Figure 1. Three radial abundance profiles used in the simulations.

namely

$$n_e = \frac{4.6 \times 10^{-2}}{[1+(\frac{r}{57})^2]^{1.8}} + \frac{4.8 \times 10^{-3}}{[1+(\frac{r}{200})^2]^{0.87}} \quad \mathrm{cm}^{-3} \tag{1}$$

and

$$T_e = 7\frac{[1+(\frac{r}{71})^3]}{[2.3+(\frac{r}{71})^3]} \quad \mathrm{keV}, \tag{2}$$

where r is measured in kpc.

For abundances we consider three possible radial behaviors – a) constant abundance, b) abundance declining with radius and c) abundance peaking at the radius of ∼50 kpc and declining both towards smaller or larger radii as shown in Fig. 1. The last functional form is closest to the radial abundance profile derived from deprojection analysis of the Chandra and XMM-Newton observations (Schmidt, Fabian & Sanders 2003, Churazov et al. 2003) under the assumption of a single temperature optically thin plasma emission model. The abundance ratios used are those of Anders & Grevesse (1989). Using these data we calculated an optical depth from the center of the cluster up to a radius of 1 Mpc $\tau = \int n_i \sigma_0 dr$, where n_i is the ion concentration and the cross section for a given ion is

$$\sigma_0 = \frac{\sqrt{\pi} h r_e c f}{\Delta E_D}, \tag{3}$$

where

$$\begin{aligned} \Delta E_{\rm D} &= E_0 \left(\frac{2kT_e}{Am_{\rm p}c^2} + \frac{V_{\rm turb}^2}{c^2} \right)^{1/2} \\ &= E_0 \left[\frac{2kT_e}{Am_{\rm p}c^2}(1+1.4AM^2) \right]^{1/2}. \end{aligned} \tag{4}$$

In the above equations E_0 is the energy of a given line, A is the atomic mass of the corresponding element, $m_{\rm p}$ is the proton mass, $V_{\rm turb}$ is the characteristic turbulent velocity, M is the corresponding Mach number, $r_{\rm e}$ is the classical electron radius and f is the oscillator strength of a given atomic transition. The wavelengths and absorption oscillator strengths are taken from the compilation of Verner, Verner & Ferland (1996). The ionization equilibrium is that of Mazzotta et al. (1998). The set of Fe lines with an optical depth larger than 0.2 (for $M = 0$) is given in Table 1. From this table it is clear that i) the 6.7 keV line of He-like iron is by far the most optically thick line for the case of pure thermal broadening and ii) strong turbulence makes resonant scattering effects negligible for all lines as was emphasized by Gilfanov et al. (1987). For other types of abundance profiles, the main result is the same – the 6.7 keV line has an optical depth of order 3 and accounting for turbulence reduces the optical depth to values smaller than 1.

Table 1. Optical depth (from $r = 0$ to $r = 1$ Mpc) to resonant scattering for a set of X-ray lines. The temperature and density profiles are give by eq. 1 and 2 above. The abundance is constant with radius at 0.5 solar. Two values are quoted – for pure thermal line broadening ($M = 0$) and for strongly turbulent gas ($M = 1$). Only the lines with an optical depth greater than 0.2 (for $M = 0$) are listed.

Ion	Energy (keV)	τ $M=0$	τ $M=1$
Fe XXIII	0.093	0.70	0.08
Fe XXIII	1.129	0.26	0.03
Fe XXIV	1.163	0.39	0.04
Fe XXIV	1.168	0.78	0.09
Fe XXV	6.700	2.79	0.31
Fe XXVI	6.973	0.20	0.02
Fe XXV	7.881	0.46	0.05

The resonant scattering has been modeled using a Monte-Carlo approach. The cluster has been divided into concentric shells and line emissivities have been assigned to each shell using the APEC v1.3.0 results (Smith et al. 2001). The scattering of photons was accounted for by assuming a complete energy redistribution and dipole scattering phase matrix. The latter assumption is motivated by the fact that we are interested primarily in the He-like iron resonant line, which has a pure dipole scattering phase matrix (see discussion in Sazonov et al. 2002). The escaping photons are accumulated into separate bins, according to their projected distance from the cluster center. The modification of the 6.7 keV line radial brightness profile due to resonant scattering (for the case of a flat abundance profile) is shown in Fig. 2. As expected, resonant scattering suppresses the line intensity in the core and raises the line intensity in the cluster outskirts. More illustrative is the ratio of the profiles with and without resonant scattering taken into account, which we show in Fig. 3 for all three abundance profile models. Inspite of the different abundance distributions, this plot shows that the net effect is very similar for all three cases – the flux in the line is suppressed by a factor of up to ∼2 within the inner 100 kpc region and is enhanced by ∼10-20% outside this region.

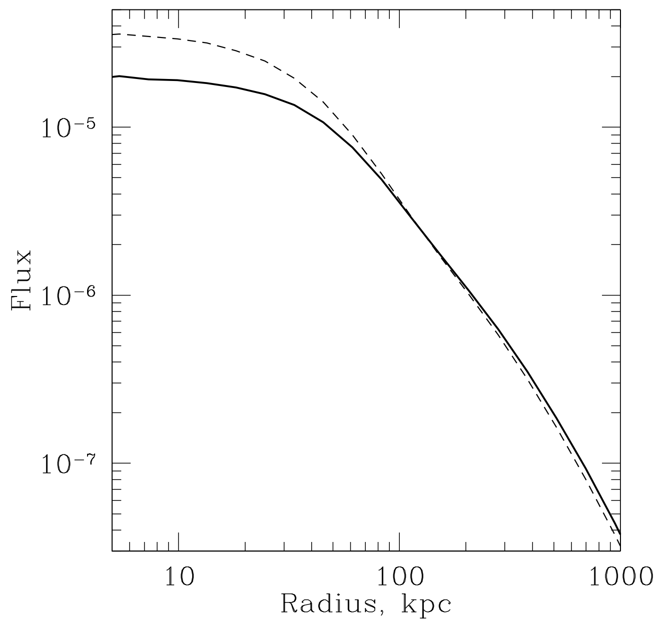

Figure 2. Radial profiles of the He-like iron K_α line (for the flat abundance profile) with (thick solid line) and without (dashed line) the effect of resonant scattering. Resonant scattering suppresses the line intensity in the core and redistributes line photons to larger radii.

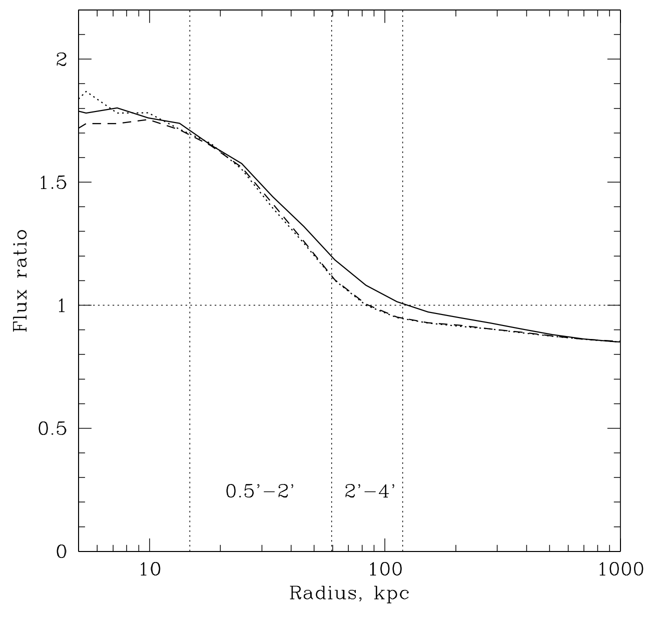

Figure 3. Ratio of the 6.7 keV radial brightness profiles without accounting for resonant scattering to the profiles including the effect of resonant scattering. Three curves correspond to three models of the abundance profiles shown in Fig. 1. Dotted vertical lines show the two regions used for spectra extraction.

3 SPECTRA

Obviously the easiest way to reveal the effect of resonant scattering is to derive the line ratios for the central region. The He-like iron K_α and K_β lines are ideally suited for that purpose since both lines are due to the same ion of iron. Guided by Fig. 3 we accumulated MOS spectra for two annuli $0.5' - 2'$ and $2' - 4'$ centered on NGC 1275. The inner $0.5'$ region was excluded in order to avoid possible contamination from the NGC 1275 nucleus. The spectrum from 5 to 9 keV was fitted with the APEC (Smith et al. 2001) and MEKAL (Mewe et al. 1986; Mewe et al. 1986; Kaastra 1992; Liedahl et al. 1995) models in XSPEC v.11.2 (Arnaud 1996) and is shown in Fig. 4. Temperature, heavy metal abundances (with the abundance ratios of Anders & Grevesse, 1989) and redshift were free parameters of the models. One can see that for the MEKAL model there is a clear excess on the left wing of the He-like iron K_β line, where the He-like nickel K_α line(s) is blended with the iron line. In order to remove this discrepancy one has to either raise the nickel abundance above the standard Ni to Fe ratio (Anders & Grevesse, 1989) by a factor ∼2 or assume that the 6.7 keV complex is suppressed by resonant scattering, thus causing peculiarities in the observed line ratio. On the other hand, the most recent APEC v1.3.0 model provides an almost perfect fit to the whole 5-9 keV portion of the spectrum. A very similar situation is seen for the spectrum of the $2' - 4'$ annulus. In what follows we assume that we can rely on the predictions of the newest APEC model, which has a significantly richer set of lines in the region of interest. The best fit temperature and abundance values for the two annuli are $T_e = 4.29 \pm 0.05$ keV, $Z = 0.501 \pm 0.007$ relative to the solar abundance (Anders & Grevesse, 1989) and $T_e = 5.18 \pm 0.06$, $Z = 0.446 \pm 0.007$. The values of temperature are somewhat higher than one would infer from fitting a broader 0.5-9 keV spectral band, which is expected for projected spectra, given the radial dependence of the temperature in the Perseus cluster (see eq. 2).

The best fit value of the abundance for the 5-9 keV spectrum is of course dominated by the contribution of the 6.7 keV line. We fixed all parameters (except abundance) at their best fit values and recalculated the abundance first ignoring part of the spectrum containing the 6.7 keV complex and second ignoring the part containing 7.9 keV complex. Since only 6.7 keV complex is affected by resonant scattering the different values of abundance in two fits would indicate an important role for scattering. The ratio of abundances calculated this way is shown in Fig. 5 with two crosses (for two annuli). Resonant scattering is expected to increase the ratio of abundances well above unity for the inner annulus. However, the observed ratio is consistent with unity, indicating that any effects from resonant scattering are small.

Finally we demonstrated that projection effects do not significantly affect the determination of the spectral parameters by using the outer $2' - 4'$ annulus as a background for the inner $0.5' - 2'$ annulus. The resulting spectrum has a somewhat lower best fit temperature ~ 3.8 keV, as one would expect, but the line flux ratio again does not show any obvious anomalies.

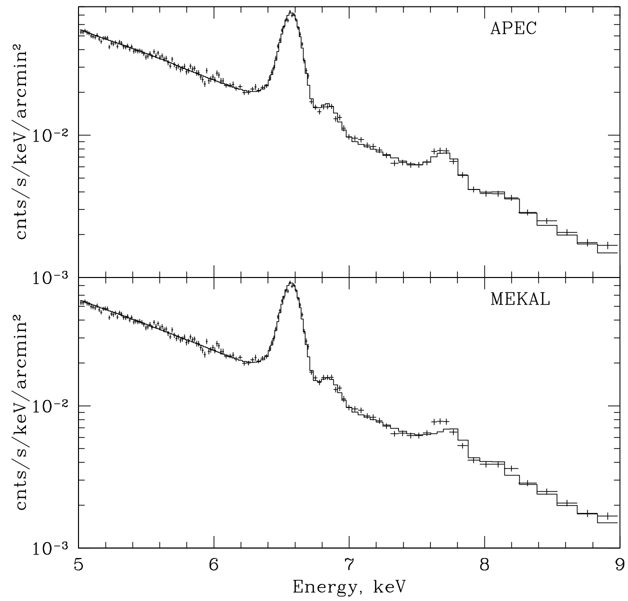

Figure 4. The 5-9 keV spectrum of the 30″ to 2′ annulus centered on NGC 1275 and fitted with APEC and MEKAL models.

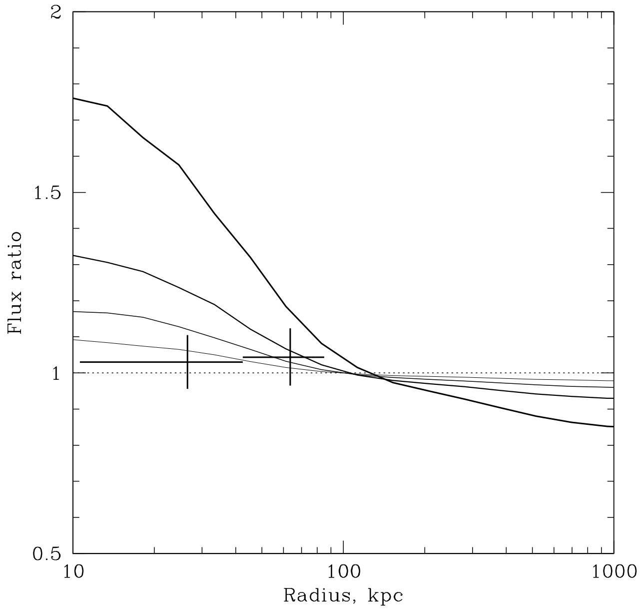

Figure 5. Influence of turbulence on the strength of the resonant scattering effect. The plot shows the same ratio as in Fig. 3 for the flat abundance profile, but calculated for Mach numbers of 0,0.25,0.5,1 (from top to bottom). For comparison, crosses show the ratio of heavy elements abundances obtained ignoring parts of the spectrum containing the 6.7 keV and 7.9 keV complexes respectively. Given that the resonant K_α line of He-like iron contributes about 50% to the 6.6-6.8 keV complex of lines, the measured abundance ratio is consistent with the curves for Mach number $\geq$0.5.

4 ROLE OF GAS MOTIONS

The resonant K_α He-like iron line contribution to the 6.7 keV (6.6-6.8 keV) complex varies from 40 to 52% for the gas temperature range from 3 to 5 keV. Therefore suppression of the resonant line flux in the inner regions due to resonant scattering would strongly affect the intensity of the whole complex. On the other hand, the 6.9 and 7.9 keV complexes can be treated as effectively optically thin. The good fit of the spectra with the APEC model of an optically thin plasma with the solar mix of heavy elements can be considered as an indication that the resonant scattering effects are suppressed. As is noted by Gilfanov et al. (1987) turbulent motions of the gas may significantly reduce the optical depth of the lines. The effect is especially strong for heavy elements, which have thermal velocities much smaller than the sound velocity of the gas. For example, for the 6.7 keV iron line, the inclusion of turbulent motions (parametrized through the effective Mach number in eq. 4) would reduce the optical depth to $\sim$0.4 for a Mach number of 1. In Fig. 5, we show the simulated ratios of the radial profiles of the 6.7 keV line with and without the effect of resonant scattering for Mach numbers of 0, 0.25, 0.5 and 1.

5 CENTRAL ABUNDANCE HOLE

Single temperature fits to the azimuthly averaged projected spectra of the Perseus cluster yield an abundance "hole" in the very core (central $\sim 1'$) of the cluster (e.g. Schmidt et al., 2002, Churazov et al. 2003). It is of course attractive to attribute this decrease in abundance to resonant scattering, since abundance measurements are mostly affected by the strongest lines which typically have the largest optical depths. The high signal-to-noise ratio accumulated during the XMM-Newton observations of the Perseus cluster allows one to make a two-dimensional map of the 6.7 keV line intensity. Shown in Fig. 6 (left panel) is the projected map of the 6.7 keV line equivalent width. The 5-8 keV band of the projected spectra was approximated as a linear combination of three components - two bremsstrahlung spectra with temperatures of 2 and 6 keV and a Gaussian line at 6.7 keV (redshifted to the cluster distance). The very central region (the circle with 20″ radius centered at NGC 1275) has been excised from the analysis to avoid contamination by the AGN flux. The equivalent width of the line was calculated by applying similar adaptive smoothings to the intensities of the line and the continuum (sum of two bremsstrahlung components) and calculating the ratio. The size of the smoothing window was chosen to provide an effective signal to noise ratio of 80, calculated using the total number of counts from 5-8 keV. The image shows (i) an overall increase in the equivalent width towards the center of the cluster, (ii) a decrease in the equivalent width in the central $\sim 1'$ region and (iii) a low equivalent width horse-shoe shaped region to the West. Since the equivalent width of the line is temperature dependent, we have calibrated this dependence using a set of simulated APEC spectra with different temperatures and a fixed heavy element abundance and applying a similar procedure for equivalent width determination. Using the resulting conversion factor (from equivalent width to abundance) and the temperature map calculated with the same adaptive smoothing procedure, we converted the equivalent width map into an abundance map - Fig. 6 (right panel). The low equivalent width region to the West of the cluster center is apparently the result of higher gas temperature in this region (see Churazov et al. 2003), since in the abundance map this feature is absent. The central "hole" is present both in the equivalent width and the abundance map, although detailed structures are different in the two maps, because of the complicated temperature structure of the inner region.

The central part ($8' \times 8'$) of the abundance map is shown in Fig. 7 along with the surface brightness image of the same region. Contours in both images show the abundance at the level of 0.4 Solar. One can see that the inner part of the abundance hole roughly traces the region occupied by the inner radio lobes (Böhringer et al. 1993, Fabian et al. 2000) which correspond to areas of low X-ray surface brightness to the North and South of the nucleus. This morphological similarity suggests that the abundance "hole" is related to the activity of the AGN rather than to resonant scattering. For instance radio lobes may push the gas with the highest abundance away from the nucleus forming a shell-like distribution of highly enriched gas. The details of the abundance distribution in this region and discussion of realistic models are beyond the scope of this paper. Given that the size of the region is rather small and there is a bright AGN at the very center, long Chandra observations would provide better data for careful study of the abundance distribution. We conclude however that a central abundance hole is not a reliable indication that resonant scattering is important in Perseus and it is likely that other physical mechanisms play a role.

6 DISCUSSION

With our parameterization of the turbulence through the effective Mach number in eq. 4, the energy in turbulent motions is approximately related to the thermal energy of the gas as $\epsilon_{turb} \approx 0.7M^2\epsilon_{th}$. A lack of visible effects of resonant scattering suggests that M is at least 0.5. Therefore turbulent motions contain at least 20% of the thermal energy of the gas. Subsonic turbulence is not very efficient in generating sound waves (e.g. Landau & Lifshitz 1963) and one can assume that a significant fraction of this energy will be dissipated locally and will go into heat. The dissipation time scale can be estimated as the eddy turn-around time times a factor f of order a few. Thus a rough estimate of the heating rate due to dissipation of turbulence can be written as:

$$\frac{\epsilon_{turb}}{f\frac{l}{Mc_s}} \approx \frac{0.7}{f}M^3\frac{\epsilon_{th}}{l/c_s} \approx \frac{\epsilon_{th}}{2\ 10^8\ yr}, \tag{5}$$

where l is the characteristic eddy size, c_s is the sound velocity. For estimates we set l = 10 kpc, M = 0.5 and f = 3. This value can be compared with the cooling rate which is set by the thermal energy and the cooling time which is of the order of 0.5 Gyr for the gas density and temperature typical of the Perseus core. Thus if the characteristic spatial scale of turbulent eddies is comparable to or less than ∼10 kpc, then the present level of turbulent dissipation should be sufficient to compensate for the gas cooling losses.

There are at least two obvious sources of turbulence – mergers and the activity of the central supermassive black hole. The numerical simulations have shown that mergers can induce long lived (of order of Gyr) eddies (e.g. Norman & Bryan 1999) even in cluster cores. The surface brightness and gas temperature structures in Perseus suggest recent merger activity (e.g. Furusho et al., 2001). The scale of merger induced eddies is probably rather large and this reduces the dissipation rate. On the other hand, activity of the supermassive black hole can induce turbulence on a smaller scales through the mechanical action of the outflows (Churazov et al. 2001,2002, Reynolds, Heinz & Begelman 2002, Brüggen & Kaiser 2002). Judging from the size of the observed radio lobes in the Perseus cluster (Böhringer et al. 1993, Fabian et al. 2000) one can expect the size of the generated eddies to be of order 10 kpc, i.e. sufficiently small to dissipate their energy quickly (compared to the timescale for radiative cooling).

The above analysis is simplified by the assumption that the same level of turbulence, expressed through the effective Mach number, is applicable to all radii. We cannot prove however with the present data that the gas velocities indeed vary on spatial scales as small as 10 kpc, nor is it possible to show that the velocity field can be characterized as turbulent motion. The conservative conclusion is therefore that the data are consistent with small scale turbulence characterized by a velocity of order half the sound speed, although larger spatial scale velocity variations (up to ∼50-100 kpc) cannot be excluded. Comparable gas velocities are found in the numerical simulations of cluster formation (e.g. Frenk et al. 1999), although the central parts of clusters with cool cores may have properties different from the bulk of the cluster gas. The profile of a resonant line, broadened by large scale motions and the turbulent cascade, has been recently calculated by Inogamov & Sunyaev (2003). While the profile differs from a simple Gaussian shape, the net effect on the optical depth in the line core is comparable. We note also that pure radial differential motions (e.g. sound waves coming from the very central region as in the picture suggested by Fabian et al. 2003) also would produce a similar reduction in the optical depth of the lines. The dissipation rate for this (predominantly radial) motion crucially depends on the viscosity of the gas (Fabian et al. 2003). For less regular motion patterns, eq. 5 gives a resonable estimate of the dissipation time scales for all values of the viscosity below a certain value (in the limit of large Reynolds numbers). For very high viscosities (low Reynolds numbers) the time scale for dissipation will be even shorter.

Assuming that the gas velocities do vary randomly on spatial scales of order 10 kpc, one can estimate the impact of these motions on the radial distribution of heavy elements. In the simplest approximation one can estimate the turbulent transport of heavy elements via the diffusion coefficient on spatial scales larger than the characteristic size of the eddies:

$$D \sim \frac{1}{3}v_t l = \frac{1}{3}Mc_s l \tag{6}$$

The characteristic time for diffusion over regions of size X e.g. 100 kpc is:

$$t \sim \frac{X^2}{D} =$$

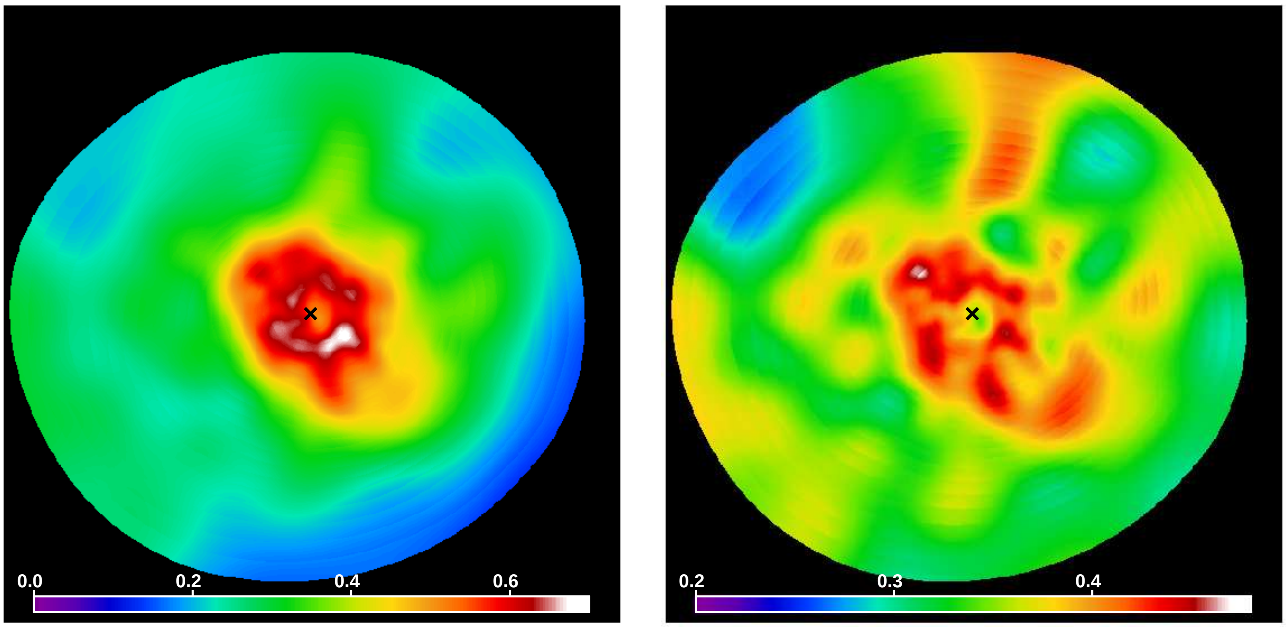

Figure 6. Left: Adaptively smoothed map of the 6.7 keV line equivalent width in units of keV. The image size is $20' \times 20'$. Cross marks the position of NGC 1275. **Right:** The abundance map (in units of Solar abundance) calculated from the equivalent width map using the projected temperature map.

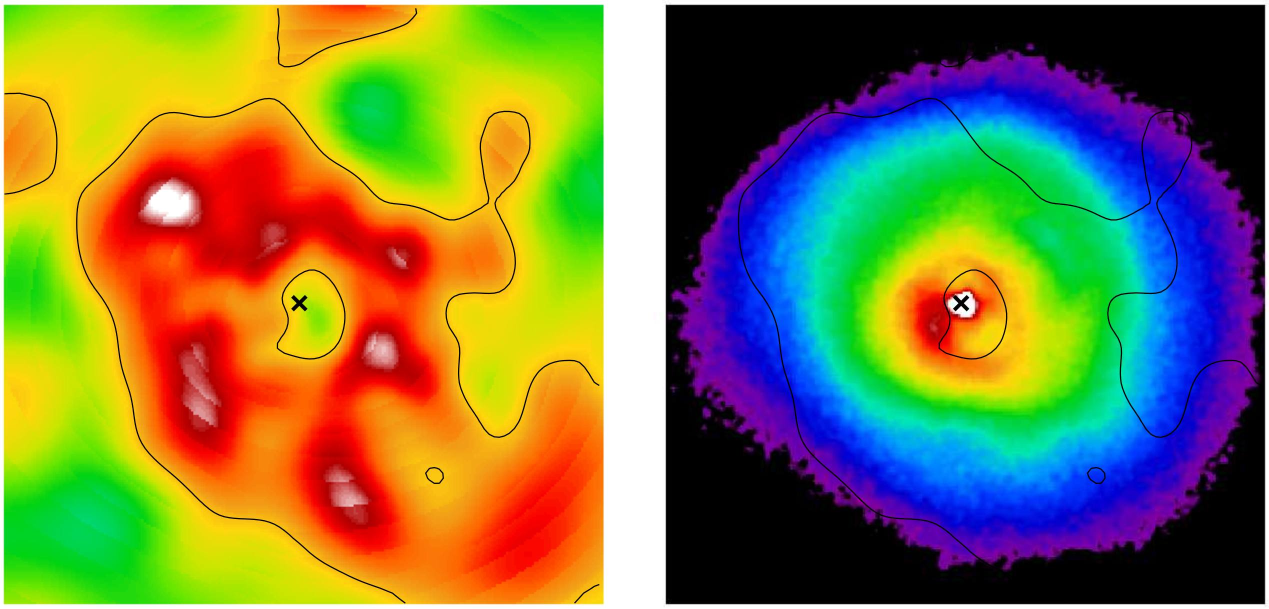

Figure 7. Left: Central $8' \times 8'$ part of the iron abundance map. **Right:** Surface brightness distribution of the same region in the 0.3-5 keV band. Contours in both images show the abundance at the level of 0.4 Solar. The inner part of the abundance hole approximately covers two regions of low surface brightness to the North and South of the nucleus that correspond to the two radio lobes (Böhringer et al., 1993, Fabian et al. 2000).

$$6 \times 10^9 \left(\frac{X}{100\ kpc}\right)^2 \left(\frac{l}{10\ kpc}\right)^{-1} \left(\frac{Mc_s}{500\ km/s}\right)^{-1}\ yr \quad (7)$$

Thus for our choice of typical eddy size and turbulent velocity, the metals are not transported outside a region much larger than 100 kpc during the lifetime of the cluster. The central abundance (adopting the abundance profile with a maximum at the center as shown in Fig. 1), however, does drop substantially on time scales of approximately 1-2 Gyr and has to be replenished by some mechanism (see Böhringer et al. (2003) for implications of abundance gradients on the properties of the cool core clusters). Given the different dependence of the turbulent diffusion coefficient (eq.7) and the rate of dissipation (eq.5) on the spatial scales of eddies and characteristic velocities, the importance of these two processes will differ. For some combinations of parameters (in particular for small eddies), the heating rate is high while the impact of turbulent transport may be limited. Since at present these values are highly uncertain, it is difficult to prove that such a situation is indeed taking place in Perseus.

The are several additional caveats associated with the above analysis which are necessary to mention. First of all there are still issues to be resolved in the plasma emission models, in particular near the He-like Ni K_α line. Compared to the MEKAL version included in XSPEC (version 11.2.0), the APEC code has an updated set of major line energies and atomic physics (Smith et al. 2001, see also **http://cxc.harvard.edu/atomdb**). For the MEKAL model, however, the best description of the spectra are obtained when Ni is overabundant (Dupke & Arnaud, 2001, Gastaldello & Molendi, 2003) rather than by effects of resonant scattering. It seems therefore that even although the predictions of two codes differ, both codes favor a minimal role for resonant scattering. Second, the presence of multi-temperature plasma in the Perseus core and projection effects make the straightforward interpretation of simple single temperature fits to the projected spectra questionable. Finally, the XMM-Newton observation of the Perseus cluster was affected by increased background (see Churazov et al. 2003 for details) which might slightly affect the spectral parameters. We believe however that all these problems should not affect our estimate that the random gas velocities in the Perseus cluster core are a substantial fraction of the gas sound speed.

The presence of differential motions and the role of the resonance scattering in the Perseus core can be verified in future X-ray observations. The most straightforward way would be the measurements of the line width with calorimeters (ASTRO-E2, Constellation-X, XEUS). Resonant lines are broadened both by the resonant scattering (e.g. Gilfanov et al., 1987) and the differential motions (e.g. Inogamov and Sunyaev 2003; Sunyaev, Norman and Bryan 2003), while the width of the forbidden or intercombination lines is affected only by differential motions. Comparison of the lines width would provide an important test on the contribution of the resonant scattering. At the temperature of 4 keV the pure Doppler width of the iron 6.7 keV resonant line is of order of 4 eV (FWHM) or $\sim$200 km/s. Resonant scattering (for an optical depth of order of 3) would double the width of the resonant line (Gilfanov et al., 1987). These values are comparable with the ASTRO-E2 energy resolution and could be measured. Shape of the line and mapping of the line centroid energy over the central region will help to identify characteristic size of the eddies (e.g. Inogamov and Sunyaev 2003).

A more demanding test for the presence of resonant scattering would be the measurements of the polarization of the line flux (Sazonov et al., 2002). The expected degree of polarization for the central region is however small (at the level of few per cents) which makes a detection or meaningful upper limits problematic for future polarimetric projects.

The third possibility is related to H_α filaments observed in the core of the Perseus cluster. If the filaments are constructed from an extremely small clouds as suggested by Fabian et al. 2003 which are dragged by the flow of the hot gas then one can get a direct estimate of the gas velocity spread $\sim 300 km/s$ (e.g. Conselice, Gallagher & Wyse, 2001) and the characteristic scales of the eddies ($\sim$ 10 kpc) from the optical data. We note that if individual clouds are not very small, have a temperature of 10^4 K and are in pressure equilibrium with the ambient hot gas at 3 10^7 K then the density contrast of $c \sim 3000$ will make them insensitive to the varying gas velocity field on the spatial scales smaller than $\sim c \times x$, where x is the size of the cloud. For instance if the size of the typical cloud is $\sim$ 1 pc, then it has to travel $\sim$ 3 kpc through the ambient gas before ram pressure will accelerate it to the velocity comparable with the gas velocity.

7 CONCLUSIONS

The Perseus cluster spectrum from 5 to 9 keV measured by XMM-Newton can be well described as emission from an optically thin plasma with solar ratios of elemental abundances, provided that the most recent version (1.3) of the APEC code is used.

The lack of any visible suppression of the He-like iron 6.7 keV line in the inner region of the Perseus cluster core implies that the optical depth of the cluster gas is significantly reduced by gas motions with velocities of order half the gas sound velocity. Dissipation of these motions may provide enough heat to replenish the energy lost from radiative cooling if the spatial scales of velocity variations are small enough (e.g. comparable to the size of AGN-inflated relativistic plasma bubbles).

8 ACKNOWLEDGEMENTS

We are grateful to Randall Smith for useful discussions. We thank the editor and the referee for important comments and suggestions. W. Forman and C. Jones thank MPA for its hospitality during their summer 2002 visits, as well as the Smithsonian Institution and Chandra Observatory for support (NASA contract NAS8-39073). This work is based on observations obtained with XMM-Newton, an ESA science mission with instruments and contributions directly funded by ESA Member States and the USA (NASA).

REFERENCES

Akimoto F. et al., 1997, in X-ray Imaging and Spectroscopy of Cosmic Plasmas, ed. F. Makino & K. Mitsuda (Tokio: Universal Academy Press), 95
Akimoto F., Furuzawa A., Tawara Y., Yamashita K., 1999, AN, 320, 283
Anders E., Grevesse N., 1989, GeCoA, 53, 197
Arnaud K.A. 1996, Astronomical Data Analysis Software and Systems V, eds. Jacoby G. and Barnes J., p17, ASP Conf. Series volume 101.
Böhringer H., Voges W., Fabian A. C., Edge A. C., Neumann D. M., 1993, MNRAS, 264, L25
Böhringer H. et al., 2003, A&A, to be submitted.
Böhringer H., Belsole E., Kennea J., et al., 2001, A&A, 365, L181
Brüggen M., Kaiser C. R., 2002, Nature, 418, 301
Churazov E., Brüggen M., Kaiser C. R., Böhringer H., Forman W., 2001, ApJ, 554, 261
Churazov E., Sunyaev R., Forman W., Böhringer H., 2002, MNRAS, 332, 729

Churazov E., Forman W., Jones C., Böhringer H., 2003, ApJ, 590, 225.
Conselice, C. J., Gallagher, J. S., & Wyse, R. F. G. 2001, AJ, 122, 2281
Dupke R. A., Arnaud K. A., 2001, ApJ, 548, 141
Fabian A. C., Sanders J. S., Ettori S., et al., 2000, MNRAS, 318, L65
Fabian A. C. et al., 2003, MNRAS, accepted
Frenk C. S., White S. D. M., Bode P., et al., 1999, ApJ, 525, 554
Furusho T., Yamasaki N. Y., Ohashi T., Shibata R., Ezawa H., 2001, ApJ, 561, L165
Gastaldello F. & Molendi S., 2003, talk at the Conference "The Riddle of Cooling Flows in Galaxies and Clusters of Galaxies", Charlottesville, May 31 – June 4, http://www.astro.virginia.edu/coolflow/abs.php
Gilfanov M. R., Sunyaev R. A., Churazov E. M., 1987, SvAL, 13, 233
Inogamov N., Sunyaev R., 2003, Astronomy Letters, in press
Kaastra J.S., 1992, An X-Ray Spectral Code for Optically Thin Plasmas (Internal SRON-Leiden Report, updated version 2.0)
Landau, L.D., Lifshitz, E.M., 1963, Fluid mechanics, Pergamon Press
Liedahl D.A., Osterheld A.L. and Goldstein W.H., 1995, ApJL, 438, 115
Mathews W. G., Buote D. A., Brighenti F., 2001, ApJ, 550, L31
Matsushita K., Finoguenov A., Böhringer H., 2003, A&A, 401, 443
Mazzotta P., Mazzitelli G., Colafrancesco S., Vittorio N., 1998, A&AS, 133, 403
Mewe R., Gronenschild E.H.B.M. and van den Oord G.H.J., 1985, A&AS, 62, 197
Mewe R., Lemen J.R. and van den Oord G.H.J., 1986, A&AS, 65, 511
Molendi S., Matt G., Antonelli L. A., Fiore F., Fusco-Femiano R., Kaastra J., Maccarone C., Perola C., 1998, ApJ, 499, 608
Norman M. L., Bryan G. L., 1999, in Lecture Notes in Physics 530, The Radio Galaxy Messier 87, ed. H.-J. Röser & K. Meisenheimer (New York: Springer), 106
Reynolds C. S., Heinz S., Begelman M. C., 2002, MNRAS, 332, 271
Sazonov S. Y., Churazov E. M., Sunyaev R. A., 2002, MNRAS, 333, 191
Schmidt R. W., Fabian A. C., Sanders J. S., 2002, MNRAS, 337, 71
Shigeyama T., 1998, ApJ, 497, 587
Smith R. K., Brickhouse N. S., Liedahl D. A., Raymond J. C., 2001, ApJ, 556, L91
Sunyaev R., Norman M., Bryan G., 2003, Astronomy Letters, in press
Verner D. A., Verner E. M., Ferland G. J., 1996, ADNDT, 64, 1
Xu H., Kahn S. M., Peterson J. R., et al., 2002, ApJ, 579, 600